

Analysis of a typical railway turnout sleeper system using grillage beam analogy

A.C. Manalo¹, T. Aravinthan^{1*}, W. Karunasena¹, and N. Stevens²

¹Centre of Excellence in Engineered Fibre Composites (CEEFC), University of Southern Queensland, Toowoomba 4350, Australia

²Nick Stevens Consulting, Pty Ltd,
Kenmore, Queensland 4069, Australia

Abstract

A simplified grillage beam analogy was performed to investigate the behaviour of railway turnout sleeper system with a low value of elastic modulus on different support moduli. This study aimed at determining an optimum modulus of elasticity for an alternative fibre composite sleeper for turnout application. The numerical simulation suggests that the changes in modulus of elasticity of sleeper, $E_{sleeper}$ and the sleeper support modulus, U_s have a significant influence on the behaviour of turnout sleepers. The increase in U_s from 10 to 40 MPa resulted in a 15% reduction in the bending moment while the increase in $E_{sleeper}$ from 1 GPa to 10 GPa has resulted in almost 75% increase in the bending moment. The shear forces in turnout sleepers is not sensitive to both the changes of the $E_{sleeper}$ and U_s while the sleeper with low $E_{sleeper}$ tend to undergo greater settlement into the ballast. An $E_{sleeper}$ of 4 GPa was found optimal for an alternative fibre composite turnout sleeper provided that the U_s is at least 20 MPa from the consideration of sleeper ballast pressure and maximum vertical deflection. It was established that the turnout sleeper has a maximum bending moment of 19 kN-m and a shear force of 158 kN under service conditions.

Keywords: Grillage beam analogy; Turnout sleepers; Modulus of elasticity; Support modulus; Fibre composites.

*Corresponding author, tel. +61 7 4631 2251; fax. +61 7 4631 2110

E-mail addresses: manalo@usq.edu.au (A.C. Manalo), aravinthant@usq.edu.au (T. Aravinthan), karunasa@usq.edu.au (W. Karunasena), stevensn@bigpond.net.au (Nick Stevens)

1. Introduction

Hardwood has been the preferred material for railway sleepers and maintenance work on existing timber sleeper track is continued to be provided by hardwoods [1]. In recent years, hardwood timber for railway sleepers is becoming more expensive, less available and is of inferior quality compared to the timber previously available. This problem has resulted in most railway industries searching for alternative materials for replacing timber sleepers. A review conducted by Manalo et al. [2] suggested that the advantages of hardwood timber sleeper can be simulated using fibre composite materials with the added advantages. Furthermore, fibre composites could be a more competitive sleeper material in specific application such as railway turnout as it has been increasingly difficult to get larger, longer and good quality hardwood timber. As the design of structures using fibre composite materials has been driven by the stiffness requirement rather than strength [3] and the cost of fibre composites are relatively higher than the traditional materials like timber, steel and concrete, it is important to ascertain the optimum stiffness of a fibre composite alternative suitable for turnout application. Such an investigation is very important to arrive at the best possible sleeper section that will satisfy both strength and serviceability requirements.

Turnout is a part of the railway where track crosses one another at an angle to divert a train from the original track [4]. Special sleepers laid on a turnout are called turnout sleepers [5]. A turnout consists of individual sleepers with varying lengths and fastening locations [6]. Because of the special nature of the turnout sleepers, their manufacturing procedure is different from that of the mainline sleepers which makes their maintenance more costly. The turnout sleepers are also produced with larger dimensions than the mainline sleepers to cope with the complex loadings due to the crossing of the train. It is important therefore to understand how the turnout sleepers respond to these forces to efficiently design an alternative sleeper from fibre composite materials. However, the complex structure of a

railway turnout system makes the analysis of the behaviour of the turnout sleepers more complicated than the mainline sleepers.

Several researchers have analysed the railway track as a beam on elastic foundation and their results showed a very good agreement between the theoretical and the experimental results [7]. Kohoutek [8] analysed the railway sleeper as a longitudinal beam resting on an elastic foundation which is loaded by a pair of equivalent static load representing the train. In such a model, the contribution of the rail and the adjacent sleepers is represented by a distribution factor which is applied to the wheel load to determine the equivalent static load. This distribution factor is based on the type of rail gauge and the spacing of the sleepers [9]. The investigation conducted by Shahin [10] concluded that a 3-dimensional finite element analysis rather than a 2-dimensional simulation is a more accurate method to investigate the behaviour of a ballasted railway foundation, but the higher number of elements using this method greatly increased the computational effort. A 2-D beam model which further accounts for variation of subgrade within the length of individual sleeper was developed by Kohoutek and Campbell [11]. This model, which statically analyses the sleeper on elastic foundation, has the possibility to investigate different lengths, different ballast moduli or different parts of the sleepers with different sectional properties.

Shokreih and Rahmat [12] investigated the effects of Young's modulus on the response of railway sleepers as there are many materials being used for railway sleepers. In their work, sleepers were modelled as beams on Winkler's elastic foundation with a constant foundation modulus. The results showed that when the modulus of the beam is higher than that of the foundation, changing Young's modulus of the beam has little effects on the response of the sleepers but has considerable effects for lower modulus. Similarly, Shahu et al. [13] indicated that sleeper support modulus can change dramatically with track construction and this variation can have greater influence on the behaviour of sleepers. Further investigation

conducted by Ticoalu [14] showed that using higher support modulus will create smaller rail seat bending moment on the turnout sleepers. These studies have shown that the analysis of beams on elastic foundation has been employed extensively and has been found to be appropriate for analysing railway structures. The results of these studies have also indicated that the bending rigidity and the sleeper support modulus directly influence the behaviour of railway sleepers. However, the finite element analyses of the abovementioned studies are implemented using only a single railway sleeper. The presence of at least two sets of continuous rails which connects the sleepers makes the inclusion of the entire turnout essential in the analysis. For this reason, the behaviour of turnout sleepers should be determined for a group of sleepers instead of a single sleeper, as the contribution of the neighbouring sleepers should be taken into account due to the joining effects of the rails.

In this study, a simple and rational structural model which considers the rail, sleeper, ballast, and subgrade in a railway turnout system is developed. The model also considers the effect of the adjacent sleepers on the behaviour of turnout sleepers through the rails secured to the sleepers. Subsequently, the response of the sleepers due to wheel load of a train passing in a railway turnout is investigated. The behaviour of sleepers with different moduli of elasticity and the influences of changes in the support modulus in the performance of turnout sleepers are analysed. Furthermore, the effect on the behaviour of timber turnout sleepers when one of the sleepers is replaced with a fibre composite sleeper to simulate the spot replacement maintenance strategy is investigated. The result of this parametric investigation could lead to an optimised section for an alternative composite sleeper in a railway turnout.

2. Theoretical model for railway turnout

A railway turnout consists of a number of sleepers and rails acting together. Thus, the AS 1085.14 [6] suggests that the turnout sleepers can be analysed by a more complex grillage

model. However, there has been no reported study on the use of such a model to analyse a railway turnout in the literature. The commonly available literature on grillage system is on the analysis of slabs, foundations and complex bridge structures. Tan et al. [15] introduced the grillage analysis method for vehicle-bridge interactions to study the dynamic effects of a moving vehicle on bridge structures. The bridge structure is modelled as a grillage assembly consisting of several longitudinal girder members and transverse beam elements. The results of their analyses showed that the grillage beam simulations represented the response of the whole bridge structure under moving loads with satisfactory accuracy. In another study, Eamon and Nowak [16] combined the grillage model of the bridge deck with solid elements to analyse the resisting effect of the secondary elements such as diaphragms, barriers and sidewalks on the load carrying capacity of the bridge structural system. The ultimate capacity predictions based on the simplified grillage model were found to be within 3-6% of the more detailed finite element models but with significantly reduced solution time. Furthermore, Fujikubo [17] used a sandwich-grillage model to analyse the linear and nonlinear hydroelastic response of very large floating structures. In his model, the top and bottom deck plates of the floating structures are modelled by rectangular membrane elements, while the bulkheads are modelled by beam elements. The results of his analyses showed that the grillage analogy is effective for the stress analysis of detailed structures or for the progressive collapse analysis of global structures. More recently, Al-Saidy et al. [18] investigated the effect of damaged steel girder on the overall behaviour of short span composite bridge system using the grillage method of analysis. The results of their analyses showed that the grillage model using STAAD III structural analysis software provided results comparable with those from a more accurate three-dimensional finite element analysis.

The abovementioned studies showed that the grillage beam system has been used extensively by several researchers to analyse complex structures because of its simplicity.

Thus, a similar model was developed in this study using Strand7 finite element software package [19] to investigate the effect of various parameters on the behaviour of sleepers in a railway turnout. The railway turnout track system is modelled as a grillage beam system consisting of simple beams and beams on an elastic foundation.

3. Railway turnout geometry

A standard 1 in 16 right-hand turnout geometry consistent with the existing Australian railway using 60 kg/m rail and a narrow gauge rail line (1067 mm) commonly used in Queensland, Australia is considered [20]. Distance between rail centres is taken as 1137 mm and the spacing of sleepers is 600 mm on centres. Sleeper dimensions were set at 230 mm x 150 mm in consideration of the replacement of deteriorating timber turnout sleepers [21]. The typical range of sleeper support modulus, U_s is taken as approximately 10 to 40 MPa [6, 9]. A combined vertical design load factor, j (including quasi-static and dynamic) as large as 2.5 is used as recommended by AS1085.14 [6] to account for the dynamic affects of travel speed combined with track and wheel irregularities. The recommendation from the AS2758.7 [22] for the maximum contact pressure at the sleeper-ballast interface of 750 kPa was also adopted. Table 1 details the components of the track structure and Fig. 1 shows the schematic diagram for a turnout sleeper. After consulting with railway industry partners, a loading configuration shown in Fig. 2 was adopted. In this figure, R_1 represents the rail seat load at the middle wheel set while R_2 corresponds to the front and the rear wheel sets. This loading pattern simulates an axle load of 25 tonnes for a typical heavy axle load common in most Australian railway lines. These 3 sets of wheel load are moved through the turnout trucks to determine the location of the most critical sleepers.

4. Finite element model of the railway turnout

A simplified three dimensional grillage model consisting of longitudinal and transverse beam elements has been developed to analyse the behaviour of railway turnout structure. The model consists of the rails, sleeper plates, sleepers, ballast, and subgrade. The finite element model considers the rails as long beams continuously supported by equally spaced sleepers. The model consists of a total of 107 sleepers including 10 transition sleepers before the switch and after the longest sleeper as shown in Fig. 3. The transition sleepers are provided to ensure that the wheel load is sufficiently distributed over several sleepers when the train enters and leaves the turnout. Sadeghi [23] suggested that the effects of wheel loads are negligible for sleepers located more than 5 m or 10 sleepers away from the load points. The sleepers are laid perpendicular to the through tracks with increasing lengths from the switch until two standard length sleepers could be placed under the through and divergent tracks. In the model, the sleeper ends have lengths of 0.58 m. The overall length of the modelled track is 61.8 m with sleeper lengths varying from 2.3 m to 4.1 m.

Strand 7 [19] finite element program is used to model the railway turnout system. The rails and the sleepers are modelled as a grillage beam system with the sleepers resting on an elastic foundation (Fig. 4). The guard and check rails are omitted to further simplify the modelling procedure. The turnout model is assumed to be in a flat terrain and the effect of irregularities on the track and wheels and the dynamic effect are assumed to be represented by the dynamic load factor. The beams are subdivided into reasonable number of elements to achieve more accurate results. A total of 1339 Beam2 elements and 1046 nodes representing the rails, sleeper plates and sleepers were used in the turnout model. The model uses one beam element for the rail per sleeper bay and (n_r+1) beam elements for the sleeper, where n_r is the number of rails supported by the sleepers. As the exact cross-section of the 60 kg/m steel rail [24] cannot be defined in Strand7 using only 2D beam element, an approximate steel

I-section with an almost equivalent moment and torsional inertia was used for the rail. Table 2 lists the section properties of the 60 kg/m steel rail. The assigned cross-section to the switch blades is similar to that of the standard rails. The sleepers were considered isotropic beams with a homogenous cross section. The sleepers are identified by numbering them from 1 to 107 starting from the front of the model as shown in Fig. 3.

In the model, the centroids of the rail and sleepers are offset with a distance equal to the sum of half their depths as shown in Fig. 5a. The beam elements were used to connect the rail and the sleepers, which were placed at the level of their respective centroids (Fig. 5b). These beam elements are modelled with an axial stiffness of 310×10^6 N/mm in compression which is equivalent to that of the 19 mm thick double shoulder level base rolled-steel sleeper plate used for 146 mm rail base [25]. In tension, the beam elements are modelled with an axial stiffness of 130×10^3 N/mm equivalent to the static vertical stiffness of timber screw spikes [26]. Only the equivalent static wheel load acting on the vertical direction is considered with no lateral and longitudinal loads. The 3 sets of wheel load shown in Fig. 2 were applied directly to the rails. The support provided by the ballast and subgrade is modelled as an elastic foundation with a combined effective support modulus using Winkler foundation model [27] in Strand7. Dahlberg [28] suggested that this model is acceptable for static loading of railway track on soft support, like tracks with timber sleepers. In this model, the element formulation for beam on elastic foundation is based on thin beam theory where transverse shear deformation is ignored. This model also assumed that the reaction of the foundation is linearly proportional to the lateral deflection of the beam.

5. Parametric study

A parametric study was conducted to determine the behaviour of sleepers in a railway turnout with varying elastic modulus resting on materials with different sleeper support moduli. The

axle load configuration in Fig. 2 was placed on sleepers 1 to 107 simulating the passing of the train to determine the location of the equivalent static wheel load that will cause the maximum bending moments, shear forces and vertical deflection on the sleepers.

5.1 Equivalent quasi-static wheel load

The AS 1085.14 [6] states that the distribution of axle loads on the turnout could be determined using the same method used for standard sleepers. Similarly, a number of analytical models developed around the world represents the vehicle by a single bogie with two symmetrical wheel masses [29]. The magnitude of this equivalent static force transmitted through the wheel load of a train is calculated following the procedures suggested in AS1085.14 [6] and the impact force caused by the train passing through the turnout is considered by the vertical design load factor.

In the AS1085.14, the axle or vertical load P , is a significant factor in the calculation of the design load for sleeper design. In this study, 25 tonnes axle load is used. The magnitude of the equivalent design static wheel load, Q (in kN) carried by each rail is computed as:

$$Q = (P/2) \times 9.81 \quad (1)$$

Rail seat load, R is calculated as a function of the design static wheel load, the combined vertical design load factor (j) and the axle load distribution factor (DF) which corresponds to rail section and sleeper spacing. This gives:

$$R = jQ(DF) \quad (2)$$

The wheel impact load has been simplified as quasi-static load in order to evaluate the response of sleepers due to the passing of a train in a turnout. A combined vertical design load factor, j of 2.5 is applied to the rail seat load, R_1 while a vertical load factor of 1.5 is applied on the front and the rear seat loads, R_2 . In the calculation of rail seat load for the FE

model of the railway turnout, a distribution factor of 1 is used as the axle load is distributed to the sleepers through the continuous rails. This has resulted in an equivalent quasi-static wheel load of around 310 kN for R_1 and 185 kN for R_2 . It is important to note that the quasi-static load of 310 kN is comparable to the highest impact force observed by Leong [30] in the actual railhead from passing train with 26 to 28-tonne axle loads. This wheel load was moved along the turnout (beginning at sleeper number 1 up to sleeper number 107) to investigate the influence of wheel load as it travels through the turnout and to determine the location of the most critical sleepers.

5.2 Sleeper support modulus, U_s

Sleepers have an important role of distributing the load from rails to the ballast [12]. The ballast then transmits the load to the subgrade and elastically absorbs the deformations induced by the sleepers. The modulus of the ballast and the subgrade supporting the sleepers can change dramatically with track construction and this variation can have greater influence on the behaviour of railway sleepers. Shahu et al. [13] indicated that the deflections of the rails were most influenced by the sleeper support modulus. Similarly, the sleeper support modulus has a significant influence on the load distribution and sleeper deflection [31]. However, it is very difficult to determine the quality of the sleeper support modulus as it requires a thorough investigation of the trackbed comprising a full assessment of the ballast, sub-ballast and formation condition [32]. In railway design, it is usually assumed that the ballast, subballast and subgrade are represented by a single element with equivalent ballast/subgrade stiffness [29]. To evaluate the effect of the different U_s , the behaviour of sleepers in a railway turnout was examined under four typical values of sleeper support modulus, 10 MPa to 40 MPa as indicated in AS 1085.14 [6] and Jeffs and Tew [9].

In the numerical simulation, the turnout sleepers were modeled as isotropic beams on elastic foundation that supports the sleepers continuously along its length. The support modulus was varied from 10 to 40 MPa, with increments of 10 MPa. In the Strand7 model, the sleeper support modulus was applied as a beam support attribute at the midpoint position of the beam. Similarly, the stiffness of the elastic support was set as compression only. This type of support enables the sleepers to effectively rest on a support with the specified stiffness when the sleepers is pushed onto it but free to move (the support is removed) when the beam is pulled away from the support. In order to determine the behavior of turnout sleepers, the sleeper support modulus is assumed uniform throughout the entire turnout model and is adjusted stepwise for all the investigated elastic moduli of sleepers.

5.3 Modulus of elasticity of the sleeper, $E_{sleeper}$

The bending stiffness of the sleepers can significantly influence the response of the railway track [33]. For the same cross section of sleeper, the bending stiffness varies according to the type of material used which has different moduli of elasticity. When a fibre composite railway sleeper is used as a replacement sleeper, it is important that this sleeper has similar strength and stiffness characteristics as the existing timber sleepers to avoid uneven distribution of loading forces. However, developing a higher bending stiffness for a fibre composite sleeper requires significant amount of fibres which could be very expensive as it requires more fibres. Thus, the minimum stiffness that would not significantly affect the behaviour of railway turnout sleepers could result in an optimum design for fibre composite alternatives. Therefore, different sleeper elastic moduli, $E_{sleeper}$ supporting the railway track were investigated. Only the lower range of the modulus of elasticity (1 to 10 GPa) were considered with the objective of developing a fibre composite railway sleeper to replace timber sleepers. This range of $E_{sleeper}$ is reasonable as most of the currently developed fibre

composite sleepers are produced with stiffness of not more than 8 GPa [34]. Furthermore, Ticoalu [14] indicated that the existing timber turnout sleepers in the Australian railways can have an elastic modulus of as low as 7 GPa.

5.4 Spot replacement of timber sleeper

The interest in replacing timber sleepers in the existing railway track with other materials has been stimulated by the increased scarcity of quality timber [35]. Currently, several railway infrastructure industries are replacing only the deteriorated sleepers in the railway track (spot replacement) to reduce the cost of maintenance. This maintenance practice leads to a situation where in the existing timber sleeper track, the replacement sleeper will be of different material and possibly different performance characteristics in service. In a study conducted by Birks et al. [36], they found out that when steel sleepers are used to replace a deteriorated timber sleeper, the steel sleepers was taking a much reduced load compared with the adjacent timber sleepers. Higher deflections were also recorded for the steel sleeper showing a lower support being supplied to the railway track at the steel sleeper installations. In another study, Kohoutek [37] found a variation between the performance of concrete and timber sleepers. He concluded that this variation is caused by the different materials of sleepers mixed in the track. The differing height of the timber sleeper to that of the concrete resulted in the load not spread evenly among the sleepers. When a fibre composite is used as a replacement sleeper, it is important that this sleeper closely matches the dimensions and the overall stiffness of the existing timber sleepers to minimise the uneven distribution of forces.

The effect on the behaviour of a railway turnout timber sleeper when the most critical sleeper is replaced with a lower $E_{sleeper}$ is investigated. Only the load case where the wheel load produces the highest positive bending moment, shear and deflection in the turnout sleepers was considered. In the analysis, four higher values of $E_{sleeper}$ for timber sleeper; 10,

15, 20 and 25 GPa were considered with the U_s kept constant at 20 kPa. These values represent the elastic modulus of the existing railway timber turnout sleepers in the Australian railway lines [14]. In the numerical simulation, the $E_{sleeper}$ is kept constant throughout the railway turnout with only the most critical sleeper replaced with a low $E_{sleeper}$ even though in actual, the sleepers in a section of a track are a mixture of sleepers of various ages and with different elastic moduli.

A summary of the design parameters is listed in Table 3. In the table, the *All FRP sleeper* represents the simulation where the all the $E_{sleeper}$ in the turnout is changed from 1 to 10 GPa with increments of 1 GPa while the U_s is varied from 10 to 40 MPa with increments of 10 MPa. On the other hand, the *Spot replacement* represents the simulation where only the most critical sleeper in the railway turnout system is replaced with a low $E_{sleeper}$.

6. Results of the parametric study

The results of the numerical simulations of the behavior of railway turnout sleepers with different combinations of elastic and support moduli are presented here..

6.1 Influence of train route on sleeper behaviour

The influence of train route in the magnitude and position of the maximum bending moment in a railway turnout sleeper is investigated. The wheel load is passed through the railway turnout in both the through (main) and the diverging tracks to determine if there is significant difference on the behavior of the railway sleepers in either of the two routes. Fig. 6 shows the maximum positive bending moment in sleepers along the through and diverging routes for railway sleepers with $E_{sleeper}$ of 10 GPa on U_s of 10 MPa. In the figure, *Case 1* represents the envelope of the maximum bending moment in sleepers when the wheel load is passing through the main track while *Case 2* is when the train is passing through the diverging track.

The results of the numerical simulations show that the turnout sleepers are subjected to an almost similar magnitude of maximum bending moments for both train routes. This is due to the arrangement of rails with respect to the sleeper essentially symmetric when the wheel load is placed either in the main or in the diverging tracks. A slightly higher bending moment was however observed on the transition sleepers after the wheel load has passed the longest sleeper for the diverging route compared to the main route which could be due to the curve rails supporting the sleepers. After the longest sleeper, the symmetry of the track is lost, implying that the tracks at the main and the diverging routes have different stiffness. In general, the difference in the influence of train routes on the behavior of sleepers is relatively small for both the main and the diverging routes. Thus, the parametric investigation to determine the effects of the different elastic and subgrade moduli on the behavior of turnout sleepers was conducted only for the model where the train pass through the diverging tracks.

6.2 Behavior of sleepers with different elastic and support moduli

The effects of the $E_{sleeper}$ on the behavior of *All FRP sleepers* are summarized in Table 4. In the table, $+BM$ and $-BM$ represent the maximum positive and negative bending moments, respectively while $+V$ and $-V$ represent the maximum positive and negative shear in the sleepers. Only the behavior of sleepers on U_s of 10 and 40 MPa are presented to illustrate the effect of the different $E_{sleeper}$ on the bending moment, shear force and vertical deflection.

a. Bending moments in sleepers

The plot of the maximum positive and negative bending moments in sleepers due to 3 sets of symmetrical wheel load of a train (in Fig. 2) placed onto rails in the diverging route of the railway turnout is shown in Figs. 7 to 10. The results of the FE model show that the maximum positive bending moment occurred under the rail seat region where each axle is placed for both the transition and the turnout sleepers. The magnitude of the positive bending

moment is higher for $E_{sleeper} = 10$ GPa than $E_{sleeper} = 1$ GPa. The results also show that the positive bending moment increases as the wheel load passes the switch but decreases before the frog. The lower bending moment at the frog could be due to the high stiffness of the rail at this section which increases its load-distributing effect. For all $E_{sleeper}$ and U_s considered, the maximum positive bending moment occurred in the turnout sleeper located between the switch and the frog.

The maximum negative bending moment can be at the rail centre or at any place along the sleeper. The location of the maximum negative bending moment occurred at the rail centre for transition sleepers and for turnout sleepers before the wheel load passed the frog. Just before passing and after the frog, the maximum negative bending moment in the turnout sleepers occurred under the rail seat of the through tracks. This could be due to the presence of the continuous rails which acted as fixed supports to the other sleeper ends creating the negative bending moment. For lower $E_{sleeper}$, the load is carried mostly by the stiffer rail and not the more flexible sleepers resulting in a lower negative bending moment while the higher $E_{sleeper}$ resulted in a higher moment due to the wheel load being carried only by a fewer sleepers. It is important to note that in all the simulations conducted, the maximum bending stress in the rails did not exceed 215 MPa. This bending stress is within the accepted stress levels of 250 MPa or 0.6 times the proof stress of the rail material as recommended by AS1085.1 [24]. The maximum negative bending moment in sleeper was again observed at the rail seat centre when the wheel load passed through the longest sleeper.

Fig. 7 shows that the maximum positive bending moment at the transition and turnout sleepers for all U_s when $E_{sleeper} = 1$ GPa. The magnitude of the positive bending moment increases when the wheel load enters the turnout. When $E_{sleeper} = 10$ GPa, the positive bending moment in the transition sleepers is around 12.1 kN-m for all the investigated U_s as shown in Fig. 8. The magnitude of the positive bending moments again increases when the

wheel load enters the turnout. Similarly, a higher bending moment was observed in lower U_s than in higher U_s . The highest positive bending moment occurred at sleeper 42 for all the investigated support moduli.

Figs. 9 and 10 show that the influence of the support modulus on the sleeper's negative bending moment is similar to that of the positive bending moment. There is an increase in the magnitude of the negative bending moment when the elastic modulus of the sleeper increases. A higher negative bending moment was also observed for lower U_s when $E_{sleeper} = 1$ GPa (Fig. 9). The negative bending moment at the transition sleepers ranges from 2.54 kN-m to 4.46 kN-m when $E_{sleeper} = 10$ GPa (Fig. 10). The negative bending moment on the sleepers increases when the wheel load enters the turnout.

The numerical analyses show that the maximum bending moment when $E_{sleeper} = 1$ GPa is not greatly different from each other for all investigated U_s but has a noticeable difference when $E_{sleeper} = 10$ GPa. Moreover, it can be seen that the bending moment in the longer turnout sleepers is more sensitive to the changes in the U_s than the shorter transition sleepers. This finding is similar to that of Namura et al. [38] where they indicated that the sleeper length has a great influence on its bending moments. The results further indicated that as the sleeper support becomes stiffer there is an increase in the magnitude of the maximum bending moment in the sleepers. Obviously, increasing the value of U_s leads to an increase in the rigidity of the foundation. As a result, the wheel load is distributed only to a fewer sleepers increasing the bending moment experienced by sleeper directly under the load.

b. Shear forces in sleepers

The shear forces are critical for beams subjected to high concentrated loads. In a railway turnout, the change in direction of a passing train causes the maximum shear to occur at the sleepers. Figs. 11 to 14 show the relationship of the maximum shear force in sleepers resting

on different U_s due to the applied wheel load on the railway turnout. The results show that the magnitude of shear force does not vary significantly with all the investigated support moduli. Only a slight increase in the maximum shear force was observed with increasing U_s .

Figs. 11 and 12 show a significant increase in the magnitude of positive shear force when the wheel load travels from the transition to turnout sleepers. The highest positive shear force calculated in the turnout sleeper has a magnitude of around 155 kN which occurred when the wheel load, R_l is seating on sleeper 13. The magnitude of the maximum shear force decreases as the wheel load travels between the switch and the frog. However, an increase in the maximum shear force was again recorded in sleeper 76 just after the wheel load passed the frog. It is important to note that the highest positive shear force in sleepers 13 and 76 occurs in the region between the through and divergent tracks. The magnitude of this shear force is up to 2.5 times higher than the transition sleepers. This high magnitude of shear force at the switch and the frog can be attributed at the flangeway opening which causes high shear forces in the sleepers. In this location, the train wheel has to “*jump*” on the flangeway opening which subjected the sleepers to the high, concentrated wheel forces. After the wheel load has passed through the sleeper at the frog, the magnitude of the shear force decreases as it enters through the divergent tracks.

Figs. 13 and 14 show that there is no significant difference on the magnitude of the highest negative shear force in all the investigated U_s . After passing the switch, an increasing magnitude of maximum shear force was observed in the turnout sleepers. In both $E_{sleeper} = 1$ GPa and 10 GPa, the maximum negative shear force occurred at sleeper 68. Fig. 13 indicates that the maximum negative shear at the transition sleepers is around 53 kN while in the turnout sleepers is around 94 kN when $E_{sleeper} = 1$ GPa. The higher $E_{sleeper}$ resulted in the wheel load distributed to only a few sleepers generating a higher shear force to the supporting sleepers. The maximum negative shear at the transition sleepers is around 59 kN while the

maximum negative force in the turnout sleepers is around 130 kN when $E_{sleeper} = 10$ GPa (Fig. 14). This high magnitude of negative shear force in the sleeper occurs at the sleeper region between the inner rails of the through and the divergent tracks. A decreasing magnitude of the negative shear force was then observed after the wheel load has passed the frog to a magnitude similar to that of transition sleepers before the wheel load enters the turnout.

c. Vertical deflection of sleepers

Figs. 15 and 16 present the vertical deflection of sleepers for all U_s considered when $E_{sleeper} = 1$ GPa and 10 GPa, respectively. The FEM results show that the maximum settlements of the sleepers occurred under the rail seats when the wheel load, R_l is placed directly over the sleeper. It can be seen clearly from the figures that the vertical deflection of sleepers decreases as the support modulus increases. The lower settlement of sleepers between the switch and the frog is due to the presence of rails between the rail seats which prevented the settlement of the sleepers. However, the effect of the rails decreases as the length of the sleeper increases as seen by the high vertical deflection of the longer sleepers. For both $E_{sleeper} = 1$ GPa and 10 GPa, there is a considerable vertical deflection of sleepers resting on $U_s = 10$ MPa but decrease significantly for $U_s = 20$ MPa or higher.

The vertical settlement of sleeper decreases as the wheel load enters the switch but increases again after the switch. In general, an increasing deflection was observed as the length of the sleeper increases with low deflection in the sleepers between the switch and the frog. The lower settlement of sleepers in this location could be due to the presence of a rail between the rail seats which acted as a support to lessen the settlement of the sleepers. After the frog, the vertical settlement increased again as the sleepers behaved more like a cantilever beam with the rails on the through tracks acting as supports. Figs. 17 and 18 show the scaled up deflected shape of a turnout sleeper when the wheel load is placed after the frog and

before the longest sleeper. As can be seen from the figures, the maximum vertical deflection in sleeper occurred under the rail seat. The results of the FEM analysis also show that the settlement of the sleepers into the ballast is slightly higher under the outer rail seat than under the inner rail seat after the wheel load has passed the frog. This is due to asymmetric loading on longer sleepers when the wheel load is passing through the divergent tracks while the other sleeper end tends to lift due to the elastic foundation. However, this upward deflection on the other end of the sleeper is restricted by the continuous rails on the main tracks. For $E_{sleeper} = 1$ GPa, the sleeper ends where the wheel load is placed deflected to its maximum while the other end deflected very minimally as the stiff rails in the main tracks are preventing the more flexible sleepers (Fig. 17). For $E_{sleeper} = 10$ GPa, the maximum deflection is again observed in the sleeper ends where the wheel load is placed (Fig. 18). Due to the higher stiffness of the sleepers, the rails could not totally prevent the other sleeper end to deflect upward. Similarly, the combination of the rails and the higher stiffer sleepers resulted to a lesser deflection for $E_{sleeper} = 10$ GPa compared to that of $E_{sleeper} = 1$ GPa.

6.5 Behavior of turnout sleepers with a spot replacement sleeper

The most critical sleepers, sleepers 42 and 68 were assigned with a low value of $E_{sleeper}$ while keeping the $E_{sleeper}$ of the other sleepers the same to simulate a railway turnout system with a spot replacement sleeper. In the analysis, the 10 sleepers before and after sleepers 42 and 68 were included. The distribution of maximum bending moment, shear and vertical deflection among the sleepers in the railway turnout with a spot replacement sleeper are shown in Figs. 19 to 21, respectively. In these figures, *All_4*, *All_10*, *All_15*, *All_20*, and *All_25* represent the railway track supported by turnout sleepers with the same $E_{sleeper}$ while the railway track with the most critical sleeper replaced by a fibre composite sleeper with an $E_{sleeper} = 4$ GPa are designated as *4_10*, *4_15*, *4_20*, and *4_25*. The railway turnout supported by $E_{sleeper} = 10$

GPa with the most critical sleeper replaced by a very flexible or a damaged sleeper (elastic modulus of only 1 MPa) is included for comparison and is designated as O_{10} .

The results of the analyses show that the behaviour of railway turnout sleepers with the same $E_{sleeper}$ is almost identical. This is similar to results of the investigation by Ticoalu [14] wherein she found no significant difference in the maximum bending moment, shear and vertical deflection for railway turnout sleepers with an $E_{sleeper} = 10$ GPa or higher and are resting on a subgrade of 20 to 40 MPa. However, it can be seen from the figures that replacing sleepers 42 and 68 with an $E_{sleeper} = 4$ GPa has a large influence on the behaviour of a group of turnout sleepers. In Fig. 19, the results show that the sleeper directly under the rail seat load R_I has the highest bending moment. In a railway turnout supported by sleepers with the same $E_{sleeper}$, the magnitude of bending moment in sleeper 42 is around 18 kN-m while in its adjacent sleepers is around 12 kN-m. Similarly, the magnitude of the bending moment in sleeper 42 for turnout with $E_{sleeper}$ of 10 to 25 GPa is only 20% higher to the bending moment experienced in All_4 .

Replacing sleeper 42 with an $E_{sleeper} = 4$ GPa leads to a lowering overall stiffness of the railway track and therefore a reduction in the bending moment starts to occur in the sleeper just below the load. As indicated in Fig. 19, a reduction in the magnitude of bending moment of almost 30% was observed for sleeper 42 compared to a railway turnout not mixed with a lower $E_{sleeper}$ even though R_I is directly over this particular sleeper. This reduction in the bending moment in sleeper 42 is however distributed to the neighbouring sleepers as seen by the increase in the bending moment of sleepers 41 and 43. For all the investigated $E_{sleeper}$, there is no significant difference in the bending moment in the spot replacement sleeper but the increase in the bending moment in the adjacent sleepers can go as high as 20% for higher $E_{sleeper}$. On the average, the bending moment in the adjacent sleepers is 22% higher than that of sleeper 42. This result shows that a fibre composites sleeper is more effective than steel for

a spot replacement sleeper. Birks et al. [36] indicated that a steel sleeper situated immediately below the wheel load carries an almost 38% lower bending moment compared to the adjacent timber railway sleepers.

The increase in the bending moment in the adjacent sleepers in *4_10*, *4_15*, *4_20*, and *4_25* is significantly less compared to that of the adjacent sleepers when the spot replacement sleeper has a very low $E_{sleeper}$ value. Similarly, the increase in the bending moment in the adjacent sleepers in *0_10* compared to the railway turnout not mixed with a low stiffness sleeper is around 45%. This is almost similar to the observations by Zhang et al. [39] when they examined the response of a railway track with unsupported sleepers. In their numerical investigation, they represented the unsupported sleeper with a zero value for elastic modulus. The results of their investigation showed that the calculated bending moment in the neighbouring sleepers when the train passes over an unsupported sleeper is almost 40% higher compared with under normal condition. Furthermore, the maximum bending moment in the sleepers 41 and 43 for *0_10* is slightly higher than that of sleeper 42 in the normal railway track. This should not be the case especially when the sleeper is designed based on the maximum bending moment acting on the sleepers for a track with a constant elastic modulus. This increase amount of bending moment taken by the adjacent sleepers might result in its early in-service failure. Interestingly, the bending moment experience by the spot replacement sleeper is higher than the bending moment in *All_4* suggesting a better distribution of load among the sleepers. Thus, it can be said that the fibre composite sleepers can be used not only for spot replacement of deteriorated timber sleepers but also in the total replacement of sleepers in railway turnout.

Fig. 20 shows that sleeper 68 has the highest shear force when R_l is directly over this sleeper. For a railway turnout without a spot replacement sleeper, the magnitude of shear force in sleeper 68 is at 140 kN, which is almost 50% higher than that of the adjacent

sleepers. Considering the load is directly over sleeper 68, the shear force at the sleepers 67 and 69 are almost same. When sleeper 68 is replaced with $E_{\text{sleeper}} = 4$ GPa, the shear force in sleeper 68 decreases to around 95 kN while in the adjacent sleepers increases to 85 kN. This represents an over 30% decrease in shear force in the spot replacement sleeper but only a 20% decrease in the adjacent sleepers with the shear force among sleepers 67 to 69 differ by only 10%. A slight increase in shear force was also observed in the neighbouring sleepers. In the evaluation of Kohoutek [37] between the performance of a railway track with mixed timber and concrete sleepers, he found out that the distribution is 30% to timber and 35% to the adjacent concrete sleepers when the load is over the timber sleeper but over 60% for concrete sleeper when the load is directly over the concrete sleeper. This result again showed that a fibre composite sleeper distributes the load more efficiently to the adjacent sleepers than a concrete sleeper.

In Fig. 25, the results show that replacing sleeper 68 with an $E_{\text{sleeper}} = 4$ GPa did not significantly change the maximum deflection in the turnout sleepers compared to that of a railway turnout with the same E_{sleeper} . The magnitude of vertical deflection in sleeper 68 is well under 6 mm for all the considered E_{sleeper} . On the other hand, replacing sleeper 68 with a very low E_{sleeper} would result in an almost 35% increase in the deflection of the adjacent sleepers. This is almost similar to the results obtained by Lundqvist and Dahlberg [40] wherein they found that the vertical displacement of sleepers adjacent to an unsupported sleeper increase by 40%. In the earlier studies by Birks et al. [36], they have observed a deflection of 9 mm for the inserted steel sleeper compared to only 5 mm for timber when not mixed with a steel sleeper. These results further show that a fibre composites sleeper is a more effective spot replacement sleeper for timber turnout sleeper than steel and concrete.

7. Discussion

The effects of the different E_{sleeper} and varying U_s on the behaviour of sleepers in a railway turnout are discussed in this section. An evaluation was also conducted to determine if the behaviour of sleepers using the practical range of values for various track parameters satisfies the technical requirements for turnout application.

7.1 Effect of elastic and support moduli on bending moment

In the range of the studied E_{sleeper} and U_s , the highest bending moments in sleepers took place when a train is passing through a turnout. The highest positive moments occurred when load, R_l is directly on sleeper 42 while the maximum negative bending moment occurred when the load is on sleeper 52. Fig. 22 shows that the maximum positive bending moment in the sleeper occurred under the rail seat region where the axle is placed while Fig. 23 shows that the maximum negative bending moment occurred between them.

The relationship between the maximum bending moments in turnout sleepers and the E_{sleeper} for the different U_s considered is shown in Fig. 24. The magnitude of the positive and the negative bending moments increases with increasing E_{sleeper} but decreases with increasing U_s . The results show that the increase in E_{sleeper} from 1 GPa to 10 GPa has resulted in almost 75% increase in the maximum bending moment, whilst a change in U_s from 10 MPa to 40 MPa reduces the maximum bending moment by 15%. Furthermore, the influence by the changes in the U_s is less in lower E_{sleeper} than in higher E_{sleeper} . The higher bending moment on sleepers with higher E_{sleeper} is due to the greater stiffness of the railway track resulting in a fewer sleepers sharing the load. Compared to transition sleepers, the increase in the magnitude of the bending moment in the turnout sleepers is around 20% for lower E_{sleeper} but is in the order of 40-55% for higher E_{sleeper} . Another area of interest is the redistribution of the load throughout the sleeper system due to the increasing U_s as shown by a decreasing

difference in the maximum bending moment in sleepers. This is more obvious when $E_{sleeper}$ is 4 GPa or higher wherein there is no significant difference on the magnitude of the bending moment in sleepers for higher values of U_s . Similar results were obtained for spot replacement sleeper wherein the distribution of bending moment among the group of sleepers is similar for $E_{sleeper}$ of 4 GPa or higher. On the basis of the simulations performed, the fibre composite sleeper should resist minimum positive and negative bending moments of 19 kN-m and 8 kN-m, respectively.

7.2 Effect of elastic and support moduli on shear force

Fig. 25 shows the maximum shear forces in railway turnout sleepers with different $E_{sleeper}$ and U_s . In Fig. 25a, it can be seen that the positive shear force in the turnout sleepers increases with increasing $E_{sleeper}$ but became almost constant when $E_{sleeper}$ is higher than 4 GPa for all the U_s considered except when $U_s = 10$ MPa wherein a decrease in shear force was observed for $E_{sleeper}$ higher than 3 GPa. On the other hand, Fig. 25b shows that the maximum shear force increases with increasing $E_{sleeper}$. Overall, there is no significant difference in the value of highest shear force in the different $E_{sleeper}$ and U_s considered. The increase in $E_{sleeper}$ from 1 GPa to 10 GPa has resulted in only 3% increase in the positive shear force and the increase in U_s from 10 MPa to 40 MPa resulted in only 1.6% increase while the increase in $E_{sleeper}$ from 1 to 10 GPa has increased the magnitude of the negative shear force by almost 40%. The high magnitude of the shear force for higher $E_{sleeper}$ than lower $E_{sleeper}$ on higher U_s is due to the stiffer track modulus which results in the load distributed only to a fewer sleepers, thus a higher force carried by the sleeper directly under the load. Noticeably, the highest shear force occurred on sleeper located just after the switch and the crossing. In these locations, shear gets very high in turnout sleeper as the rails are close together as shown in Figs. 26 and 27. When the wheel load is placed on the diverging track, a lot of the load on one rail is carried

by the adjacent rail. The magnitude of this shear force is almost 2.5 times higher than that of the transition sleepers. This further confirms that the shear force is critical in turnout sleepers. More importantly, the results suggest that the sleepers for railway turnout application should be designed with a higher shear capacity than the mainline sleepers. The railway turnout should carry a minimum shear force of 158 kN. The result of the numerical simulation also provided information on the location of the maximum shear force along the sleeper lengths. This information is very helpful in determining where the bulk of the fibre composite materials should be placed in a turnout sleeper section for a more cost effective design.

7.3 Effect of elastic and support moduli on deflection and sleeper/ballast pressure

Fig. 28 shows the maximum vertical deflection and the ballast/sleeper pressure of railway turnout sleepers with $E_{sleeper}$ and U_s . In Fig. 28b, the contact pressure between the sleeper and the ballast is calculated by multiplying the U_s and the deflection divided by the width of the sleeper with the compressive stresses that the sleepers exert on the ballast bed are considered evenly distributed.

The analyses show that the U_s has a significant influence on the vertical deflection and the sleeper/ballast pressure. It is clearly observed that the vertical displacement of sleeper decreases with increasing $E_{sleeper}$ and U_s . The lower the U_s , the more likely the sleeper will deflect and settle into the ballast while a more uniform settlement occurs at higher U_s . This also means that sleepers with higher $E_{sleeper}$ provided more stability in railway tracks. On the other hand, the change of the U_s from 10 to 40 MPa increases the pressure between the sleeper and the ballast. This is because the U_s tries to isolate the individual sleepers in the turnout resulting in a higher load carried by the sleeper directly under the load. Thus, it can be concluded that a better distribution of the wheels load on the group of sleepers can be attained for lower $E_{sleeper}$ but this will result in higher sleeper deflection.

Fig. 28a shows that the increase in the $E_{sleeper}$ from 1 to 10 GPa resulted in a decrease in the vertical deflection of the sleepers by 23-36% for the different U_s considered. However, the results also suggest that varying the $E_{sleeper}$ from 4 GPa to 10 GPa does not make a major difference in deflection particularly for higher U_s . Similarly, the increase in U_s from 10 to 40 MPa decrease the vertical deflection of the sleepers by at least 60%. In Fig. 24b, it can be seen that increasing the $E_{sleeper}$ from 1 to 10 GPa results in 23-36% decrease in the sleeper ballast pressure. On the other hand, the increase in support modulus from 10 MPa to 40 MPa resulted in an increase in the sleeper/ballast pressure by as much as 35%. The same magnitude of increase in the sleeper/ballast pressure was observed by Shahu et al. [13] in their laboratory model test railway track when the U_s increased from 10 MPa to 50 MPa. This suggests that the grillage beam analogy to model the entire turnout system is reasonable to use as they are producing meaningful results.

The sleeper deflection under the rail is the main criterion in a railway track analysis [41]. For railway track in Australia, the maximum static deflection in a railway structure on ballasted track should be around 6.35 mm to give requisite combination for flexibility and stiffness [9]. The results indicated that except for $U_s = 10$ MPa and sleepers with $E_{sleeper}$ of lower than 4 GPa, the calculated vertical deflection in all the combinations used is within the recommended value. An $E_{sleeper} = 4$ GPa is also needed for a spot replacement sleeper for the timber sleeper turnout track to not exceed the maximum allowable vertical deflection. This result further suggests that a fibre composite turnout sleeper at 60 kg/m rail and 600 mm spacing should be supported by a foundation with as U_s of at least 20 MPa or a subgrade of at least good subsoil. Furthermore, the recommended maximum allowable contact pressure between the sleeper and the ballast of 750 kPa can only be satisfied using a turnout sleeper with an elastic modulus of at least 3 GPa. This stiffness characteristics can be easily achieved

using fibre composite materials which require less material to achieve similar performance resulting in a more competitive sleeper material.

8. Conclusion

A simplified three dimensional grillage beam model was used to investigate the behaviour of turnout sleepers with different moduli of elasticity resting on different support moduli. Turnout sleepers with modulus of elasticity from 1 to 10 GPa for all fibre composites and 10, 15, 20 and 25 GPa for spot replacement and support modulus of 10 to 40 MPa were considered. The maximum bending moment, shear force and displacement occurred in a sleeper when the wheel load is directly above that sleeper. In all the scenarios investigated, the behaviour of sleepers in railway turnout is most critical between the switch and the frog. The highest bending moment, shear and deflection are produced in this region. Compared to that of the transition sleepers, the magnitude of the bending moment and shear force in turnout sleepers is almost 180% and 250% higher, respectively.

The analyses showed that the changes in the modulus of elasticity and the ballast/subgrade stiffness have a significant influence on the behaviour of railway turnout sleepers. The bending moment in turnout sleeper is less affected by the changes in support modulus but affected significantly by the changes in modulus of elasticity of sleeper. Increasing the support modulus from 10 to 40 MPa resulted in only 15% reduction in the bending moment while the increase in sleeper stiffness from 1 GPa to 10 GPa has resulted in almost 75% increase in the maximum bending moment. The results also indicated that shear force in sleepers is not sensitive both to the changes of the modulus of elasticity and sleeper support modulus. Similarly, sleeper with lower modulus in elasticity and support modulus tend to undergo greater settlement into the ballast.

The results of the FEM analyses provided a basis for an optimum design of fibre composite turnout sleeper alternative. The results suggest that there is no significant difference in the behaviour of sleepers with elastic modulus of 4 to 10 GPa. On the basis of the simulations performed, the fibre composite turnout sleeper should be designed to carry minimum positive and negative bending moments of 19 kN-m and 8 kN-m, respectively and a shear force of 159 kN under normal service conditions. Most importantly, it was found that a modulus of elasticity for the development of a fibre composite sleeper alternative can be as low as 4 GPa provided that the support modulus is at least 20 MPa at 600 mm spacing from the consideration of sleeper/ballast pressure and the requirement for stable track for a maximum total vertical deflection. A spot replacement timber sleeper with this elastic modulus value is also more effective than steel and concrete. Furthermore, the numerical investigation provided information on the location and magnitude of maximum bending moment and shear along the turnout sleeper length which could be very useful in the design and manufacturing of a more cost-effective turnout sleeper.

The results of the numerical simulation suggest that the grillage beam analogy to model the entire turnout system is reasonable as they are producing results comparable to the complex analysis of other researchers. Therefore, the outcome of this study should be taken as a preliminary result, and a more thorough analysis including other railway turnout geometry and load conditions should be considered. The proposed numerical model for the analysis of the behaviour railway turnout sleeper also needs further calibration and verification using field-measured data.

References

- [1] Vinden, P, Torgovnikov, G, Hann, J. Microwave modification of radiate pine railway sleepers for preservative treatment. *European Journal of Wood and Wood Product* 2010; Springer Berlin / Heidelberg.
- [2] Manalo, AC, Aravinthan, T, Karunasena, W, Ticoalu, A. A review of alternative materials for replacing existing timber sleepers. *Composite Structure* 2010; 92(3): 603-611.
- [3] Gangarao, HVS, Taly, N, Vijay, PV. Reinforced concrete design with FRP composites. CRC Press, Taylor and Francis Group, Florida, 2007.
- [4] Pfeil, H, Broadley, JR. Turnouts – “The hungry asset”. *Railway Engineering Conference, Adelaide; 1991. p. 176-184.*
- [5] Andersson, C, Dahlberg, T. Wheel/ rail impacts at a railway turnout crossing. *Journal of Rail and Rapid Transit; 1998. viewed 21 May 2008,*
<<http://www.ingentaconnect.com/content/pep/jrr/1998/00000212/00000002/art00002>>
- [6] Standards Australia, AS1085.14-2003, Railway track material, Part 14: Prestressed concrete sleepers.
- [7] Hetenyi, K. Beams on elastic foundation: theory with applications in the fields of civil and mechanical engineering. University of Michigan Press, Michigan, USA, 1976.
- [8] Kohoutek, R. Dynamic and static performance of interspersed railway track. *Railway Engineering Conference, Adelaide, Australia, 1991.*
- [9] Jeffs, T, Tew, GP. A review of track design procedures: Volume 2 – Sleepers and ballast. *Railways of Australia, 1991.*
- [10] Shahin, MA. Investigation into some design aspects of ballasted railway track substructure. *Proceedings of the Conference on Railway Engineering, 7-10 Sep, Perth; 2008. p. 617-623.*
- [11] Kohoutek, R, Campbell, KD. Analysis of spot replacement sleepers. *Proceedings of the Fourth International Heavy Haul railway Conference, Brisbane, Australia; 1989, p. 316-321.*
- [12] Shokrieh, MM, Rahmat, M. Effects of Young’s modulus on response of railway sleeper. *Applied Mathematical Modelling* 2007; 31: 700-711.
- [13] Shahu, JT, Sharma, A, Sharma, KG. Numerical modelling pf railway tracks with ballast and sub-ballast layers using critical state parameters. *Proceedings of the International Conference of International Association for Computer Methods and Advances in Geomechanics (ICMAG), 1-6 October, Goa, India; 2008, p. 4400-4408.*
- [14] Ticoalu, ANE. Investigation on Fibre Composite Turnout Sleepers, Master of Engineering dissertation, University of Southern Queensland, Toowoomba, Queensland, Australia; 2008.
- [15] Tan, GH, Brameld, GH, Thambiratnam, DP. Development of an analytical model for treating bridge-vehicle interaction. *Engineering Structures* 1998; 20(1-2): 54-61.
- [16] Eamon, CD, Nowak, AS. Effect of secondary elements on bridge structural system reliability considering moment capacity. *Structural Safety* 2004; 26: 29-47.
- [17] Fujikubo, M. Structural analysis for the design of VLFS. *Marine Structures* 2005; 18: 201-226.

- [18] Al-Saidy, AH, Klaiber, FW, Wipf, TJ, Al-Jabri, KS, Al-Nuaimi, AS. Parametric study on the behaviour of short span composite bridge girders strengthened with carbon fibre reinforced polymer plates. *Construction and Building Materials* 2008; 22: 729-737.
- [19] Strand7. Strand7 Release 2.3.7 finite element analysis system. Sydney, Australia: Strand7 Software; 2005.
- [20] Railway Technical Society of Australasia (RTSA), Engineers Australia Newsletter 2, 2008.
- [21] Australian Rail Track Corporation (ARTC). Timber sleeper, turnout and bridge transom specification. ETA-02-01 Engineering (Track and civil) Standard; 2007.
- [22] Standards Australia AS 2758.7. 1996. Aggregates and rocks for engineering purposes, Part 7: Railway ballast.
- [23] Sadeghi, J. Investigation on modelling of railway track system. *Scientia Iranica* 2001; 8(1):76-79.
- [24] Standards Australia AS 1085.1. 2002. Railway track material. Part 1: Steel rails.
- [25] Standards Australia AS 1085.3. 2002. Railway track material. Part 3: Sleeper plates.
- [26] Thompson, DJ, Verheij, JW. The dynamic behaviour of rail fasteners at high frequencies. *Applied Acoustics* 1997; 52(1): 1-17.
- [27] Tong, P. Exact solutions of certain problems by finite element method. *American Institute of Aeronautics and Astronautics Journal* 1969; 7: 178-180.
- [28] Dahlberg, T. Some railroad settlement models – a critical review. *Proceedings of the Institution of Mechanical Engineers, Part F, Journal of Rail and Rapid Transit* 2001; 215(4): 289–300.
- [29] Steffens, D, Murray, M. Establishing meaningful result from models of railway track dynamic behaviour. Queensland University of Technology, Brisbane, Australia; 2005.
- [30] Leong, J. Development of a limit state design methodology for railway track. Master of Engineering Thesis, Queensland University of Technology, Queensland, Australia; 2007.
- [31] Cox, J. Deflection of sleeper in ballast. *Vehicle System Dynamics* 1995; 24(1): 146–153.
- [32] Brough, M, Stirling, A, Ghataorab, G, Madelin, K. Evaluation of railway trackbed and formation: a case study. *NDT&E International* 2003; 36: 145–156.
- [33] Grassie, SL, Cox, SJ. The dynamic response of railway track with flexible sleepers to high frequency vertical excitation. *Proceedings of the Institution of Mechanical Engineers, Part D: Transport Engineering* 1984; 198: 117-124.
- [34] Aravinthan, T, Manalo, AC, Douglas, S. Development of a fibre composite turnout sleeper. *Proceedings of CECAR/ASEC 2010*, Sydney, Australia; 2010.
- [35] Van Erp, G, Cattell, C, Heldt, T. Fibre composite structures in Australia’s civil engineering market: an anatomy of innovation. *Progress in Structural Engineering Materials* 2005; 7: 150-160.
- [36] Birks, FJ, Tew, GP, Chitty, GB. Narrow gauge track with interspersed steel sleepers. *The Fourth International Heavy Haul Railway Conference*, Institution of Engineers, Brisbane, Australia; 1989: 297-302.

- [37] Kohoutek, R. Dynamic and static performance of interspersed railway track. Railway Engineering Conference, Adelaide, Australia, 1991.
- [38] Namura, A, Kohata, Y, Miura, A. Effect of sleeper size on ballasted track settlement. Railway Technical Research Report 2004; 45(3): 156-161.
- [39] Zhang, S, Xiao, X, Wen, Z, Jin, X. Effect of unsupported sleepers on wheel/rail normal load. Soil Dynamics and Earthquake Engineering 2008; 28: 662-673.
- [40] Lundqvist, A, Dahlderg, T. Load impact on railway track due to unsupported sleepers. Proceedings of Institution of Mechanical Engineers Part F: Journal of Rail and Rapid Transit 2005; 219: 67-77.
- [41] Zakeri, J, Sadeghi, J.. Field investigation on load distribution and deflections of railway track sleepers. Journal of Mechanical Science and Technology 2007; 21: 1984-1956.

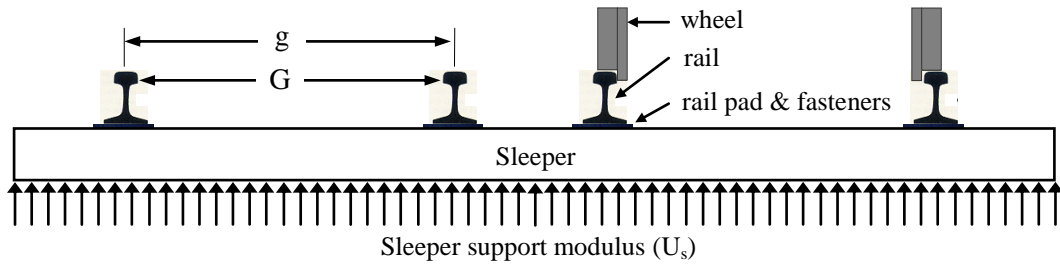


Fig. 1 Schematic diagram of turnout railway sleeper

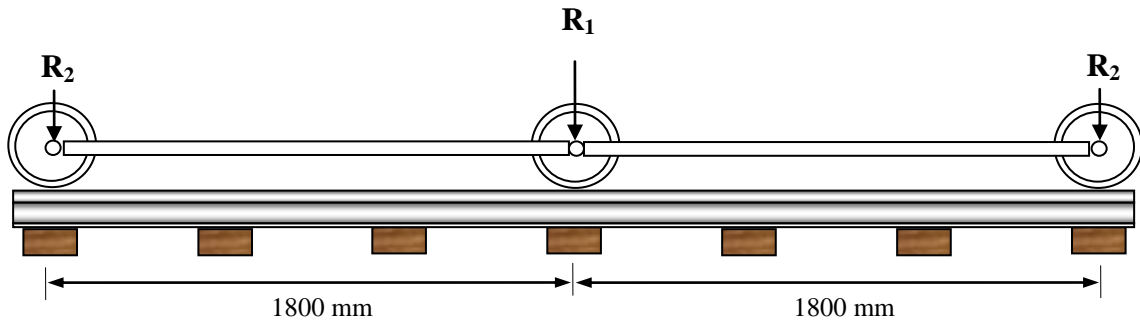


Fig. 2 Axle load configuration

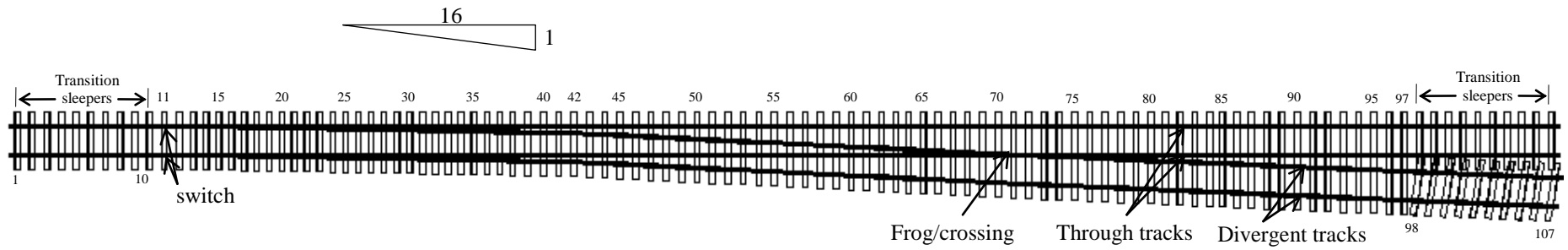


Fig.3 Geometry of a 1:16 standard right-hand railway turnout

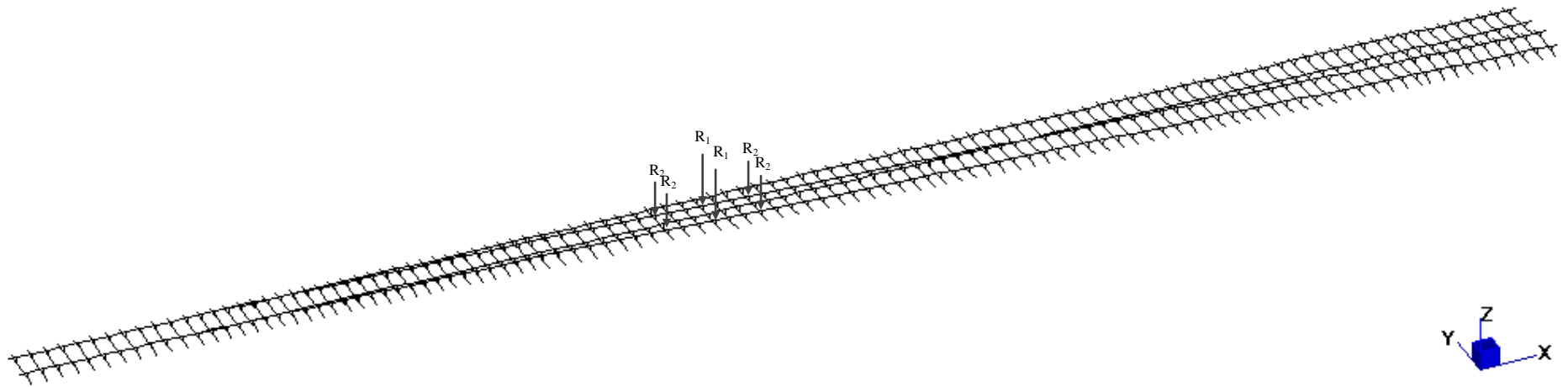


Fig.4 The grillage beam model for 1:16 standard right-hand railway turnout

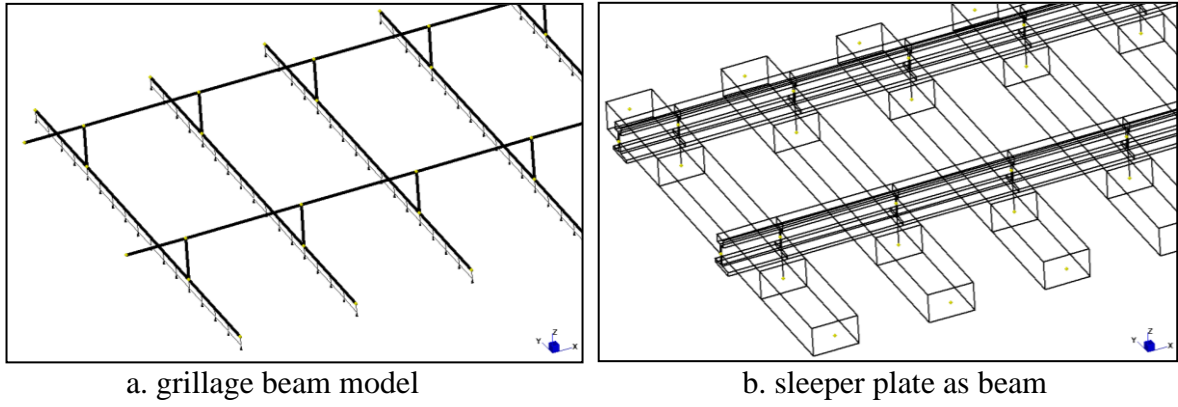


Fig. 5 Details of the turnout sleeper model

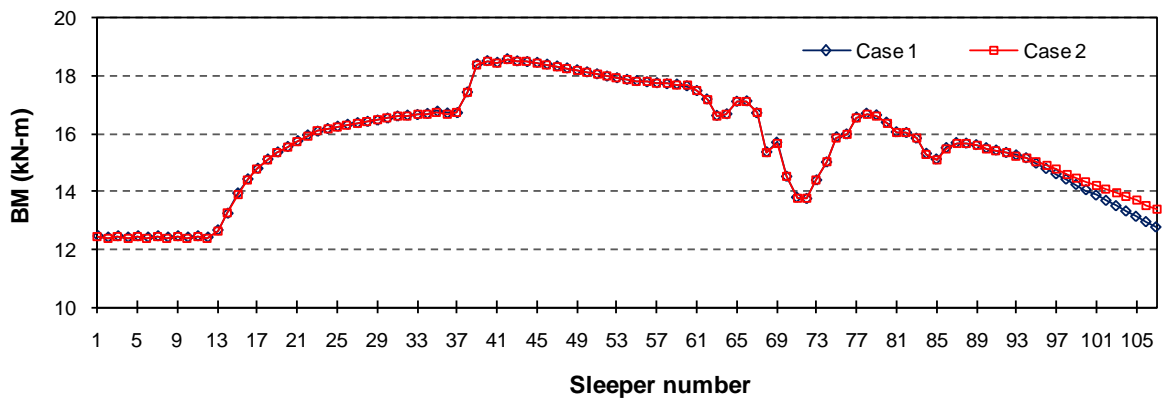


Fig. 6 Maximum bending moments on sleepers when $E_{sleeper} = 10$ GPa and $U_s = 10$ MPa

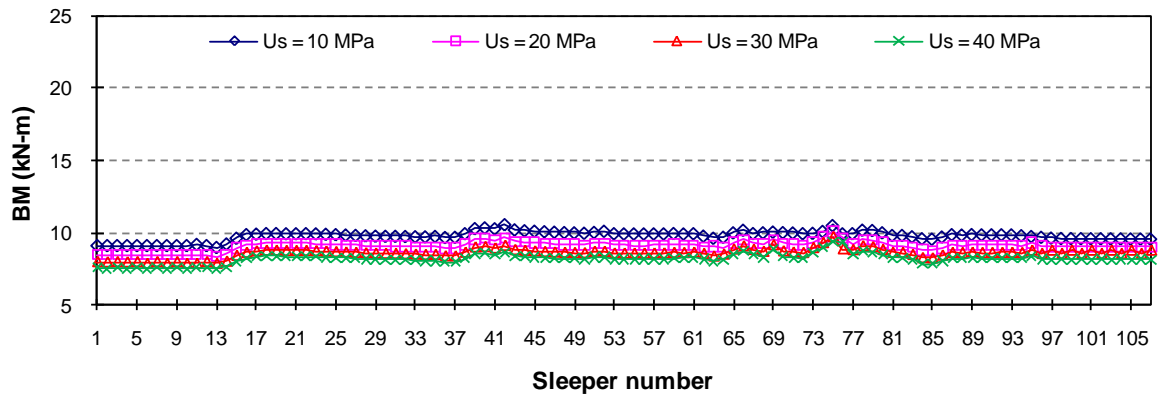


Fig. 7 Maximum positive bending moment of sleeper when $E_{sleeper} = 1$ GPa

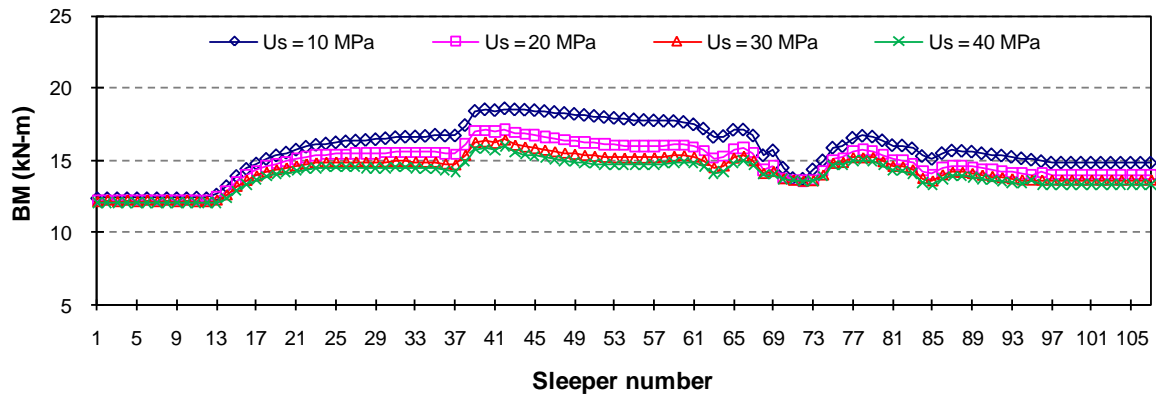


Fig. 8 Maximum positive bending moment of sleeper when $E_{sleeper} = 10$ GPa

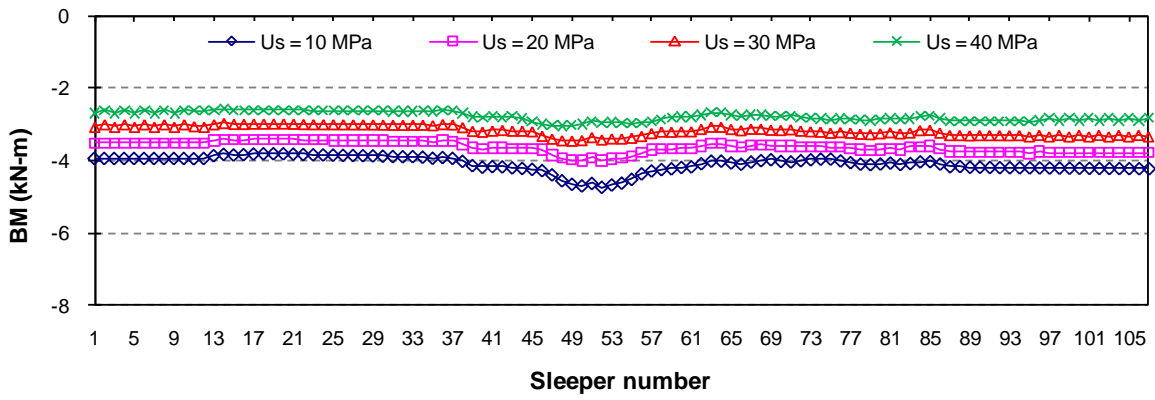


Fig. 9 Maximum negative bending moment of sleeper when $E_{sleeper} = 1$ GPa

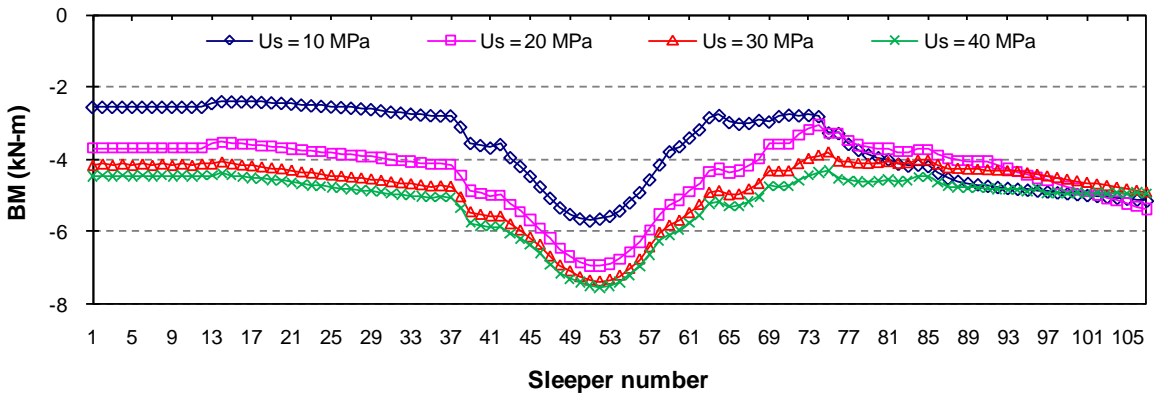


Fig. 10 Maximum negative bending moment of sleeper when $E_{sleeper} = 10$ GPa

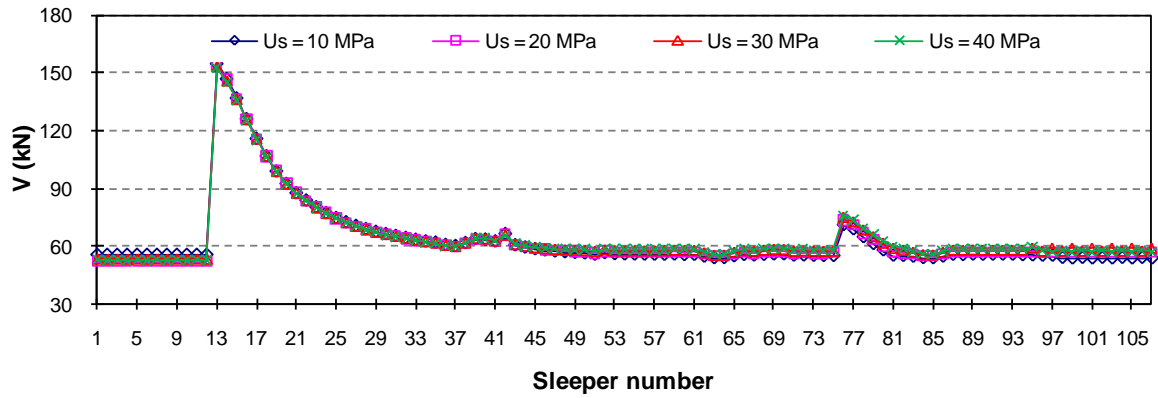


Fig. 11 Maximum shear on sleeper when $E_{sleeper} = 1$ GPa

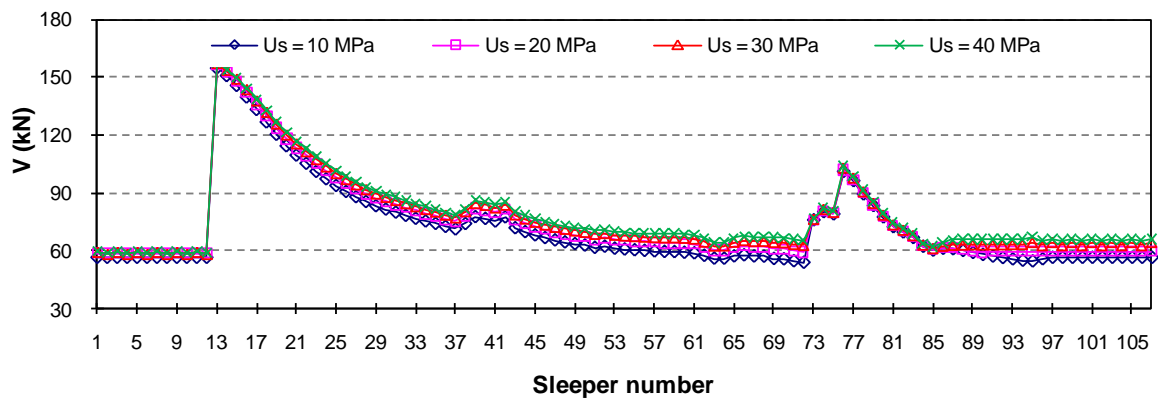


Fig. 12 Maximum positive shear on sleeper when $E_{sleeper} = 10$ GPa

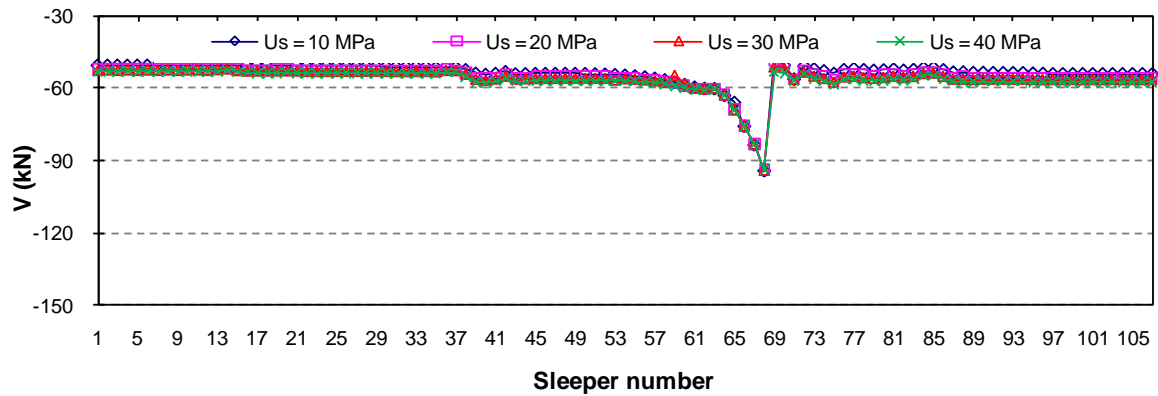


Fig. 13 Maximum negative shear on sleeper when $E_{sleeper} = 1$ GPa

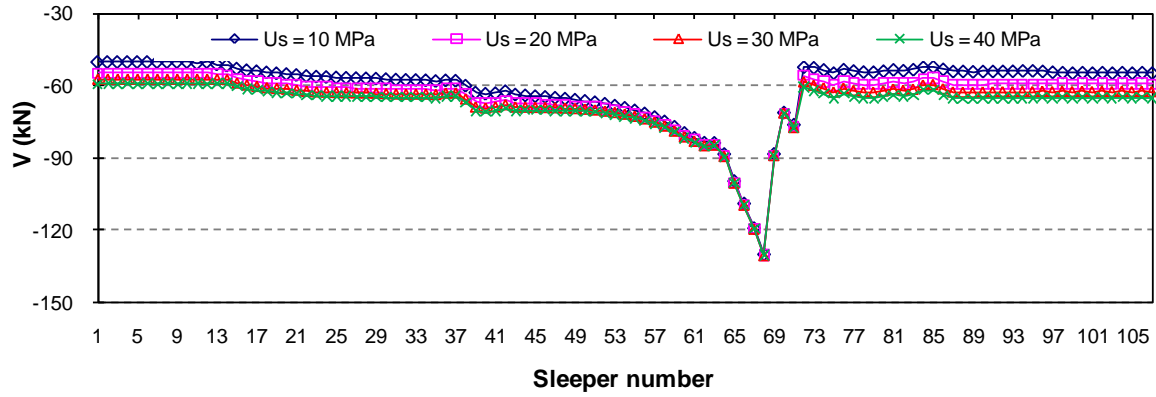


Fig. 14 Maximum negative shear on sleeper when $E_{sleeper} = 10$ GPa

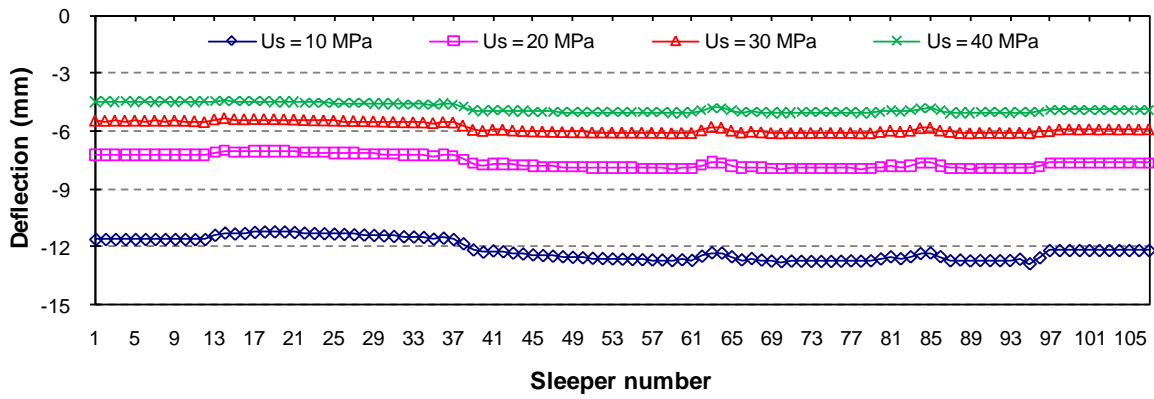


Fig. 15 Maximum deflection of sleeper when $E_{sleeper} = 1$ GPa

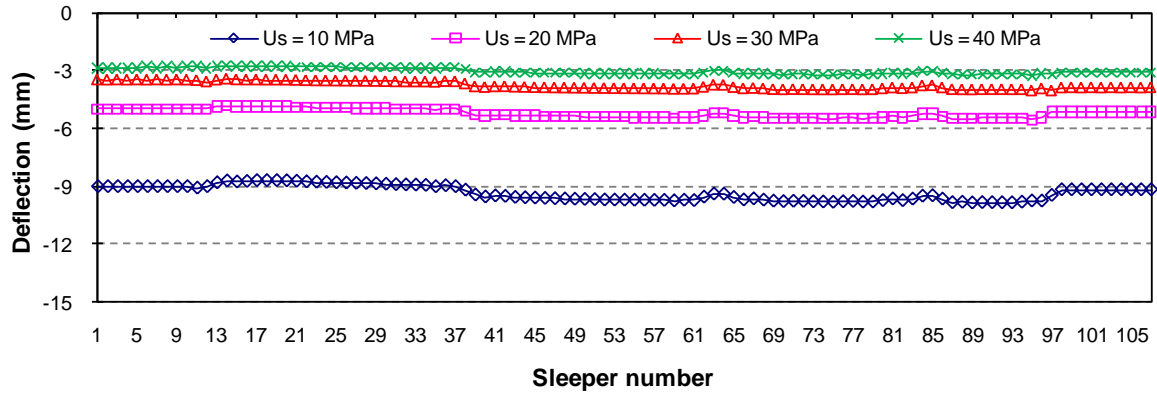


Fig. 16 Maximum deflection of sleeper when $E_{sleeper} = 10$ GPa

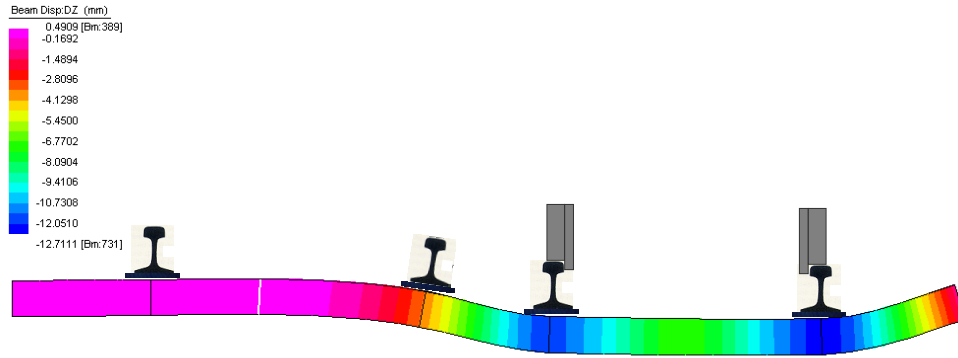


Fig. 17 Deflection of turnout railway sleepers when $E_{sleeper} = 1$ GPa and $U_s = 10$ MPa

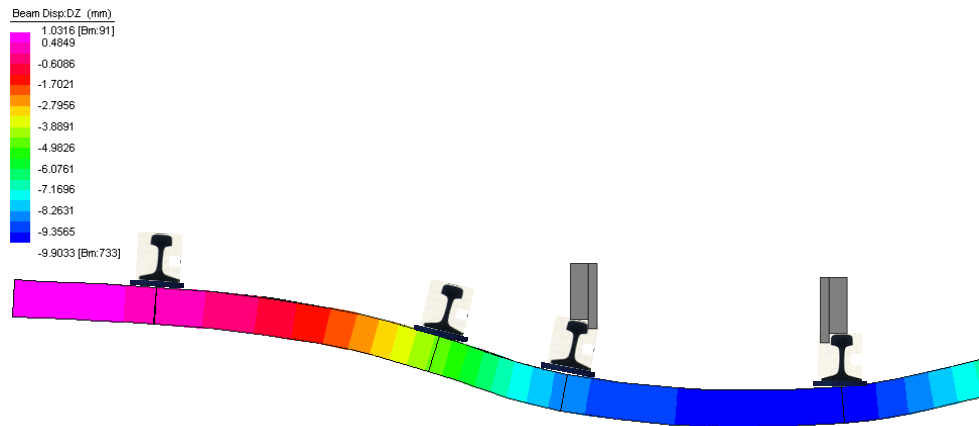


Fig. 18 Deflection of turnout railway sleepers when $E_{sleeper} = 10$ GPa and $U_s = 10$ MPa

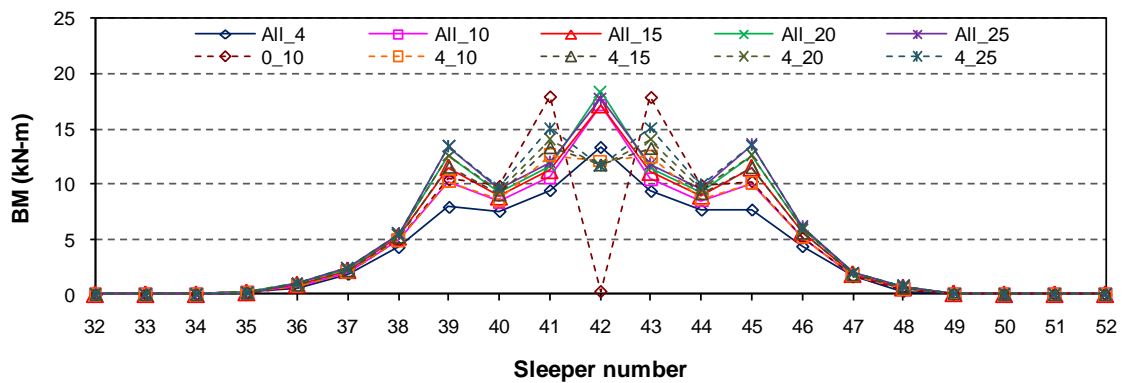


Fig. 19 Maximum bending moment in sleepers 32 to 52

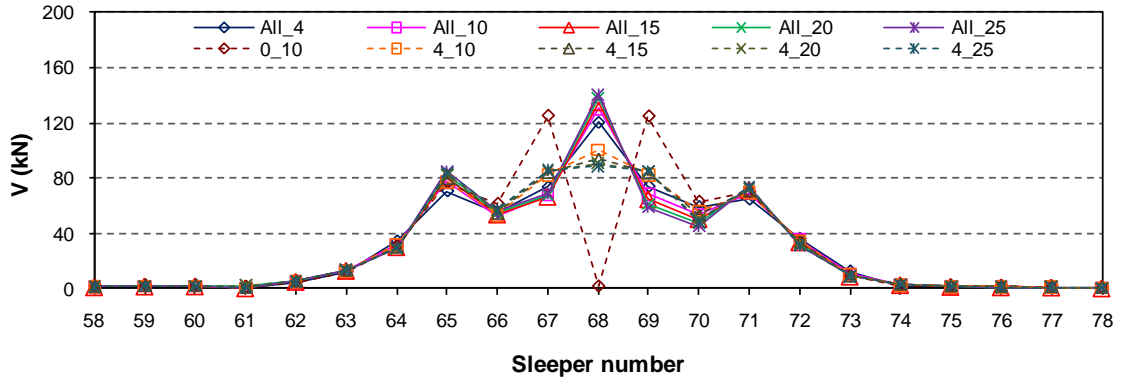


Fig. 20 Maximum shear in sleepers 58 to 78

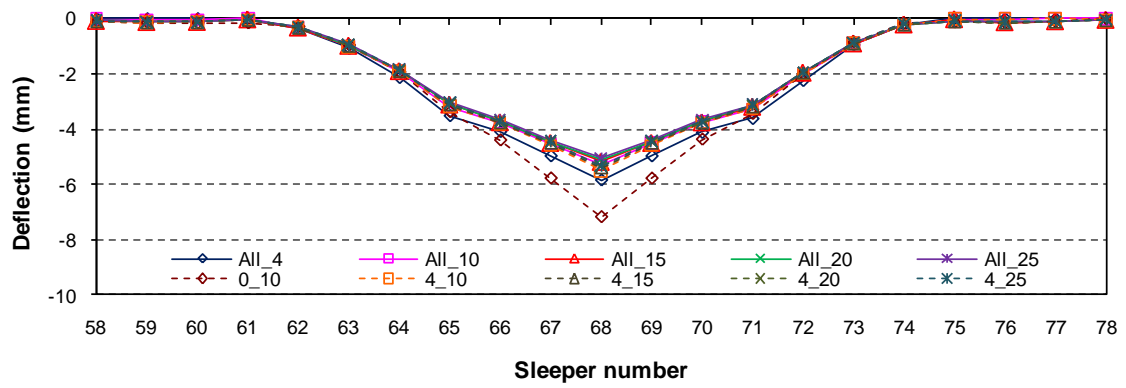


Fig. 21 Maximum vertical deflection in sleepers 58 to 78

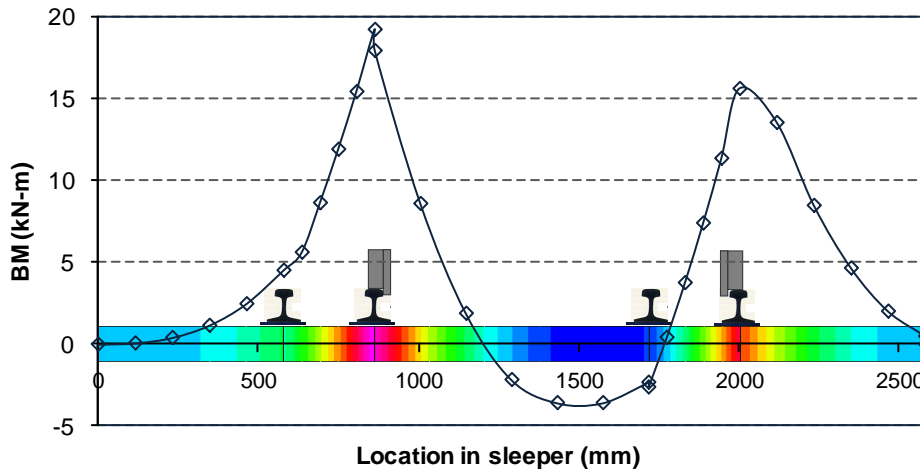


Fig. 22 Bending moment in sleeper 42

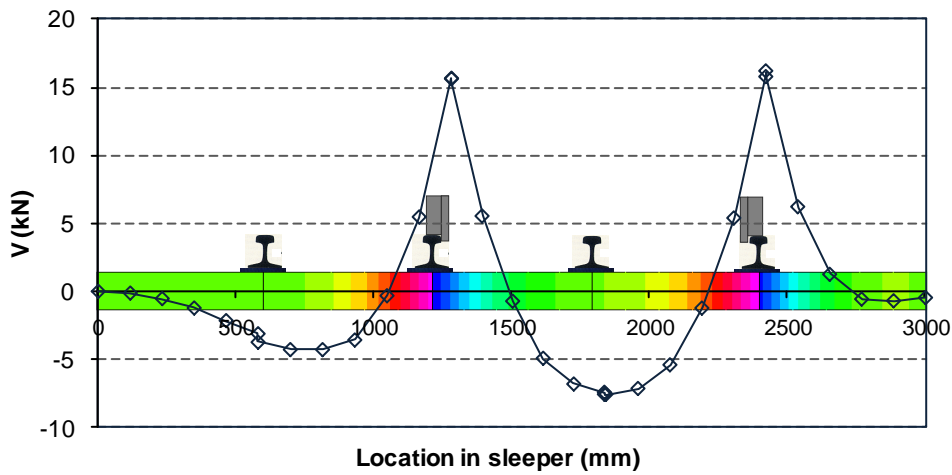


Fig. 23 Bending moment in sleeper 52

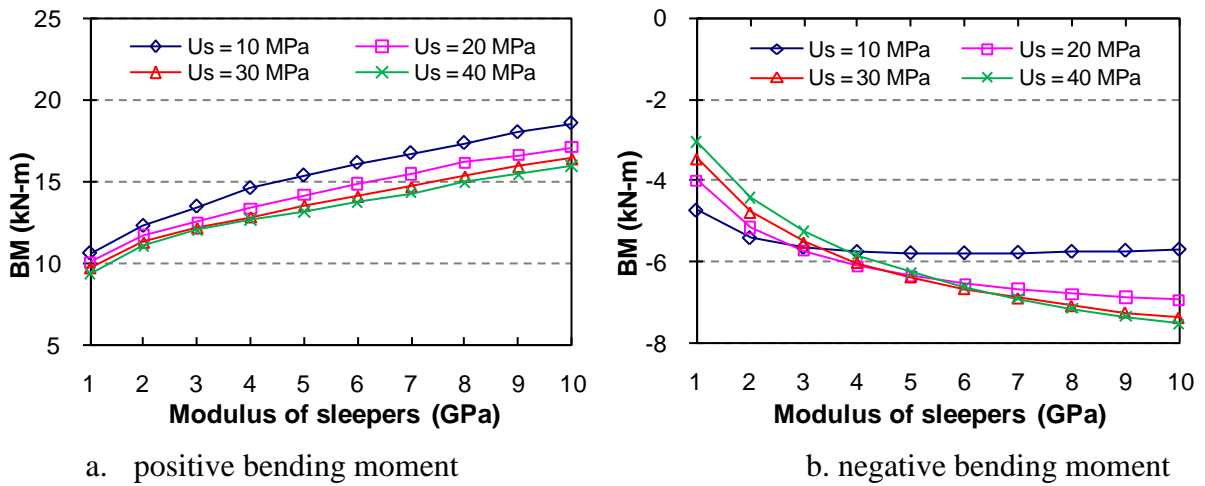


Fig. 24 Maximum bending moment in railway turnout sleepers

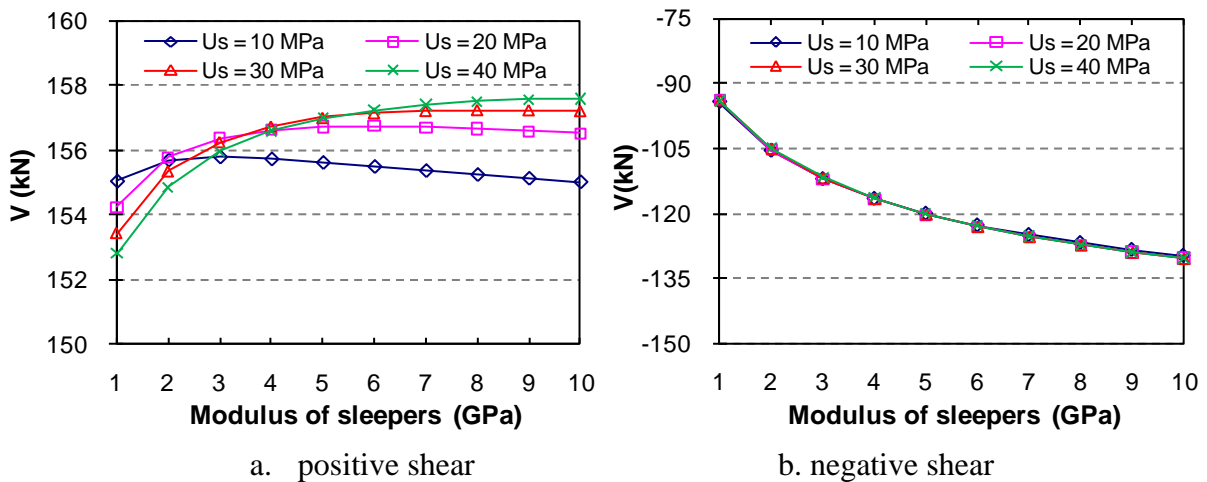


Fig. 25 Maximum shear forces in railway turnout sleepers

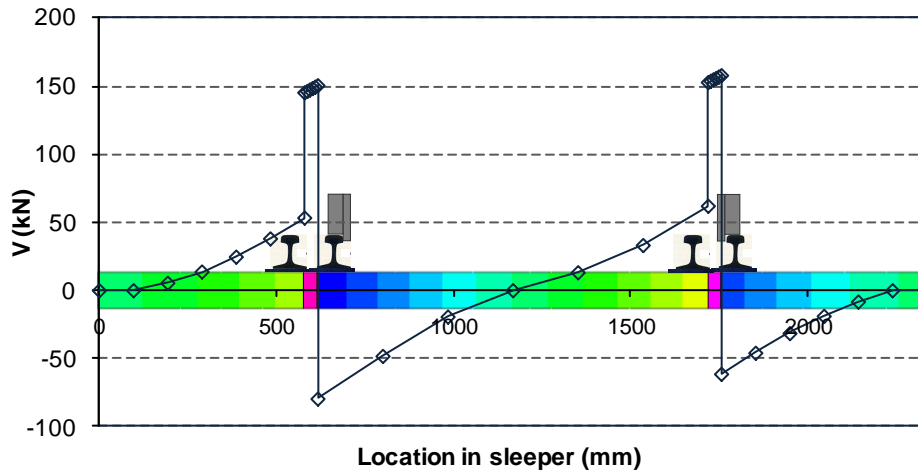


Fig. 26 Shear force envelope in sleeper at the switch

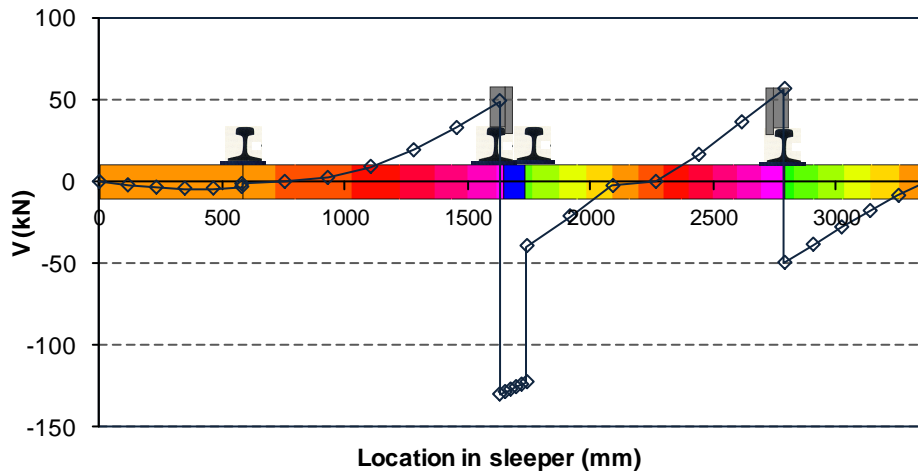
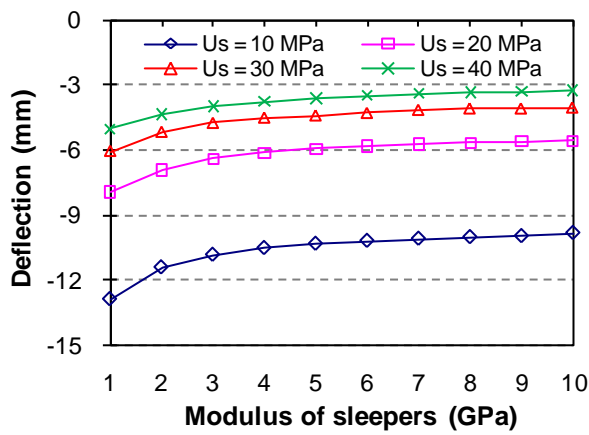
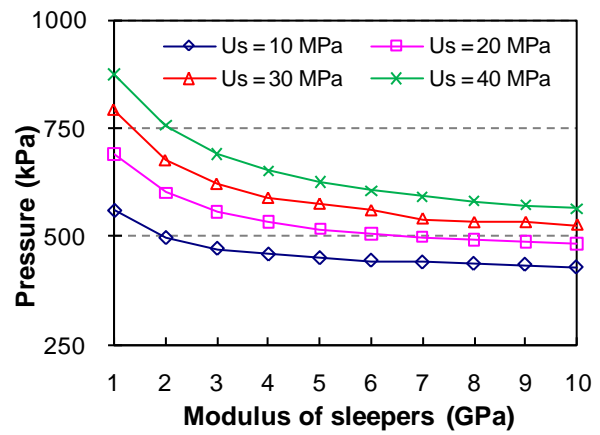


Fig. 27 Shear force envelope in sleeper at the crossing



a. Vertical deflection



b. sleeper/ballast pressure

Fig. 28 Vertical deflection and sleeper/ballast pressure

Table 1. Details of the components of the track structure

Component	Description
Rail section	60 kg/m
Rail gage (G)	1067 mm
Distance between rail centres (g)	1137 mm
Sleeper spacing	600 mm
Axle load	25 tonnes
Combined vertical load factor (j)	2.5
Sleeper support modulus (U_s)	10 - 40 MPa
Allowable ballast pressure	750 kPa
Stiffness of rails	200 GPa

Table 2. Section properties of the 60 kg/m steel rail [24]

Component	Exact	Approximate
Total area, mm ²	7.725×10^3	7.276×10^3
Second moment of inertia (I_{x-x}), mm ⁴	29.3×10^6	29.4×10^6
Second moment of inertia (I_{y-y}), mm ⁴	4.90×10^6	5.85×10^6
Section modulus head, mm ³	322.4×10^3	325.9×10^3
Section modulus foot, mm ³	369.3×10^3	368.7×10^3

Table 3. Design parameters for turnout sleeper system

Description	$E_{sleeper}$, GPa	U_s , MPa
All FRP sleepers	1 - 10	10 - 40
Spot replacement	10, 15, 20 and 25	20

Table 4. Behaviour of sleepers with different $E_{sleeper}$ and U_s

U_s (MPa)	10				40			
	Transition		Turnout		Transition		Turnout	
$E_{sleeper}$ (GPa)	1	10	1	10	1	10	1	10
+BM (kN-m)	9.1	12.4	10.6	18.6	7.6	12.1	9.4	16.1
-BM (kN-m)	3.9	2.5	4.7	5.7	2.7	4.4	3.1	7.5
+V (kN)	55.4	56.5	155.1	155.0	53.3	59.6	152.8	157.6
-V (kN)	54.1	54.8	94.3	129.8	53.1	59.3	93.9	130.4
Deflection (mm)	11.6	9.1	12.9	9.9	4.5	2.9	5.1	3.3